J|A|C|S
ARTICLES
Published on Web 06/18/2004

Sequential Oxidation of the Cubane [4Fe−4S] Cluster from $[4Fe-4S]^-$ to $[4Fe-4S]^{3+}$ in $Fe_4S_4L_n^-$ Complexes

Hua-Jin Zhai, Xin Yang, You-Jun Fu, Xue-Bin Wang, and Lai-Sheng Wang*

Contribution from the Department of Physics, Washington State University, 2710 University Drive, Richland, Washington 99352, and W. R. Wiley Environmental Molecular Sciences Laboratory, Pacific Northwest National Laboratory, MS K8-88, P.O. Box 999, Richland, Washington 99352

Received January 9, 2004; E-mail: ls.wang@pnl.gov

Abstract: Gaseous $Fe_4S_n^-$ ($n = 4-6$) clusters and synthetic analogue complexes, $Fe_4S_4L_n^-$ (L = Cl, Br, I; $n = 1-4$), were produced by laser vaporization of a solid Fe/S target and electrospray from solution samples, respectively, and their electronic structures were probed by photoelectron spectroscopy. Low binding energy features derived from minority-spin Fe 3d electrons were clearly distinguished from S-derived bands. We showed that the electronic structure of the simplest $Fe_4S_4^-$ cubane cluster can be described by the two-layer spin-coupling model previously developed for the [4Fe] cubane analogues. The photoelectron data revealed that each extra S atom in $Fe_4S_5^-$ and $Fe_4S_6^-$ removes two minority-spin Fe 3d electrons from the [4Fe−4S] cubane core and each halogen ligand removes one Fe 3d electron from the cubane core in the $Fe_4S_4L_n^-$ complexes, clearly revealing a behavior of sequential oxidation of the cubane over five formal oxidation states: $[4Fe-4S]^- \rightarrow [4Fe-4S]^0 \rightarrow [4Fe-4S]^+ \rightarrow [4Fe-4S]^{2+} \rightarrow [4Fe-4S]^{3+}$. The current work shows the electron-storage capability of the [4Fe−4S] cubane, contributes to the understanding of its electronic structure, and further demonstrates the robustness of the cubane as a structural unit and electron-transfer center.

1. Introduction

Iron−sulfur proteins are involved in a variety of vital biological processes, such as respiration, photosynthesis, and nitrogen fixation.[1−3] The active sites of these proteins normally contain iron−sulfur clusters with one to four iron atoms, among which the cubane [4Fe−4S] cluster is the most prototypical.[4] We have been interested in probing the electronic structure and chemical bonding of Fe−S clusters and complexes in the gas phase using photoelectron spectroscopy (PES). We were able to transport a variety of synthetic Fe−S analogue complexes from solution samples to the gas phase using electrospray ionization and systematically investigated their electronic properties.[5−10] In particular, we recently studied a series of doubly charged cubane-type anions $[Fe_4S_4L_4]^{2-}$ (L = SC_2H_5, SH, Cl, Br, I) and the Se-analogues $[Fe_4Se_4L_4]^{2-}$ (L = SC_2H_5, Cl) and compared the experimental data with broken symmetry density functional calculations.[10] The PES data provided the intrinsic oxidation potentials of the $[Fe_4S_4L_4]^{2-}$ complexes and their dependence on the terminal ligands. During these studies, we observed surprisingly symmetric fission in the doubly charged cubane complexes, $[Fe_4S_4L_4]^{2-} \rightarrow 2[Fe_2S_2L_2]^-$,[11,12] providing direct experimental evidence for the two-layer spin-coupling model for the [4Fe−4S] cubane core.

In the current article, we report sequential oxidation of the cubane [4Fe−4S] core in a series of gaseous cubane complexes. Bare $Fe_4S_n^-$ ($n = 4-6$) cluster anions were produced both by laser vaporization of a solid Fe/S target and collision-induced dissociation (CID) of $[Fe_4S_4(SC_2H_5)_4]^{2-}$ complexes in an electrospray source. Partially coordinated complexes, $Fe_4S_4L_n^-$ (L = Cl, Br, I; $n = 1-4$), with variable oxidation states of the cubane core were produced by CID of the corresponding $[Fe_4S_4L_4]^{2-}$ complexes in the electrospray source. The bare $Fe_4S_4^-$ cluster possesses five minority-spin Fe 3d electrons, and the $[Fe_4S_4L_4]^-$ complexes and the $Fe_4S_6^-$ cluster each have only one minority Fe 3d electrons. PES features due to the minority-spin 3d electrons were shown to lie at the lowest binding energy part of the spectra and could be readily distinguished from the S-derived PES bands. The PES spectra demonstrated a behavior of sequential oxidation of the [4Fe−4S] cubane core over five formal oxidation states: $[4Fe-4S]^-$ ($Fe_4S_4^-$) → $[4Fe-4S]^0$ ($Fe_4S_4L^-$) → $[4Fe-4S]^+$ ($Fe_4S_4L_2^-$ and $Fe_4S_5^-$) → $[4Fe-4S]^{2+}$ ($Fe_4S_4L_3^-$) → $[4Fe-4S]^{3+}$ ($Fe_4S_4L_4^-$ and $Fe_4S_6^-$). Each extra S atom in $Fe_4S_5^-$ and $Fe_4S_6^-$ was shown to remove two minority-spin Fe 3d electrons from the [4Fe−4S] cubane core,

(1) Lovenberg, W., Ed. *Iron−Sulfur Proteins, Vols. I and II.*; Academic Press: New York, 1973.
(2) Spiro, T. G.; Ed. *Iron−Sulfur Proteins*; Wiley-Interscience: New York, 1982.
(3) Cammack, R. *Adv. Inorg. Chem.* **1993**, *38*, 281.
(4) Beinert, H.; Holm, R. H.; Munck, E. *Science* **1997**, *277*, 653.
(5) Wang, X. B.; Wang, L. S. *J. Chem. Phys.* **2000**, *112*, 6959.
(6) Yang, X.; Wang, X. B.; Wang, L. S.; Niu, S. Q.; Ichiye, T. *J. Chem. Phys.* **2003**, *119*, 8311.
(7) Yang, X.; Wang, X. B.; Fu, Y. J.; Wang, L. S. *J. Phys. Chem. A* **2003**, *107*, 1703.
(8) Niu, S. Q.; Wang, X. B.; Nichols, J. A.; Wang, L. S.; Ichiye, T. *J. Phys. Chem. A* **2003**, *107*, 2898.
(9) Yang, X.; Razavet, M.; Wang, X. B.; Pichett, C. J.; Wang, L. S. *J. Phys. Chem. A* **2003**, *107*, 4612.
(10) Wang, X. B.; Niu, S. Q.; Yang, X.; Ibrahim, S. K.; Pickett, C. J.; Ichiye, T.; Wang, L. S. *J. Am. Chem. Soc.* **2003**, *125*, 14072.

and each halogen ligand removed one. It is showed that the "inverted level scheme" can be used to describe the electronic structure of the bare Fe_4S_4 clusters and the partially coordinated cubanes. Ligand-induced splittings of the minority-spin Fe 3d bands of the [4Fe−4S] cubane core were also observed as a result of different coordination environments in the two [2Fe−2S] sublayers in the partially coordinated complexes.

2. Experimental Methods

The experiments were performed with two different magnetic-bottle PES apparatuses, one equipped with a laser vaporization supersonic cluster source[13] and the other with an electrospray ionization source.[14]

2.1. PES with the Laser Vaporization Cluster Source. The experiments on bare iron−sulfur clusters $Fe_4S_n^-$ ($n = 4-6$) were carried out using the laser vaporization PES apparatus. Briefly, a mixed Fe/S target (10/1 molar ratio) was laser-vaporized in the presence of a helium carrier gas. Various $Fe_mS_n^-$ clusters were produced from the cluster source and were mass-analyzed using a time-of-flight mass spectrometer. The clusters of interest were selected and decelerated before being photodetached. Three detachment photon energies were available and used in the PES experiment on $Fe_4S_n^-$ ($n = 4-6$): 355 nm (3.496 eV) and 266 nm (4.661 eV) from an Nd:YAG laser and 193 nm (6.424 eV) from an ArF excimer laser. Photoelectrons were collected at nearly 100% efficiency by the magnetic bottle and analyzed in a 3.5 m long electron flight tube. Photoelectron spectra were calibrated using the known spectrum of Rh^-, and the energy resolution of the apparatus was $\Delta Ek/Ek \approx 2.5\%$, that is, ~25 meV for 1 eV electrons.

2.2. PES with the Electrospray Ion Source. The experiments on the $Fe_4S_4L_n^-$ (L = Cl, Br, I; $n = 1-4$) complexes were carried out using the electrospray PES apparatus.[14] Briefly, 10^{-3} M solutions of $(Bu_4N)_2[Fe_4S_4L_4]$ (L = Cl, Br, I) in O_2-free acetonitrile were sprayed through a 0.01 mm diameter syringe needle (biased at −2.2 kV) under N_2 atmosphere. The resulting charged droplets were fed into a desolvation capillary heated to ~80 °C. A negative DC voltage (~ −2 V) was applied to the skimmer after the capillary to achieve CID. Anions formed in the desolvation capillary and the CID products were guided by a radio frequency quadrupole device into a quadrupole ion trap. Ions were accumulated for 0.1 s in the trap before being pulsed out into the extraction zone of a time-of-flight mass spectrometer. The mass signals were dominated by the parent dianions $[Fe_4S_4L_4]^{2-}$ and CID fragments, which included $Fe_4S_4Cl_n^-$ ($n = 3, 4$), $Fe_4S_4Br_n^-$ ($n = 2-4$), and $Fe_4S_4I_n^-$ ($n = 0-4$). The singly charged $Fe_4S_4L_4^-$ complexes were produced by collision-induced electron detachment from the corresponding $[Fe_4S_4L_4]^{2-}$ parent dianions. $Fe_4S_4L_3^-$ can be formed by either removal of an L^- ligand from the parent dianion $\{[Fe_4S_4L_4]^{2-} \rightarrow Fe_4S_4L_3^- + L^-\}$ or Fe−L bond scission from the $Fe_4S_4L_4^-$ singly charged anion ($Fe_4S_4L_4^- \rightarrow Fe_4S_4L_3^- + L$). Subsequent CID required Fe−L bond scission from the singly charged $Fe_4S_4L_3^-$ fragment to produce the smaller $Fe_4S_4L_n^-$ singly charged fragments, i.e., $Fe_4S_4L_3^- \rightarrow Fe_4S_4L_2^- + L$. For L = Cl, we could not observe this bond scission process. But, for L = I, this process can go all the way down to the bare $Fe_4S_4^-$ cluster. Bare $Fe_4S_5^-$ and $Fe_4S_6^-$ clusters were also produced from CID of $[Fe_4S_4(SEt)_4]^{2-}$ from electrospray of a $(Bu_4N)_2[Fe_4S_4(SEt)_4]$ solution.

The fragment anions of interest, i.e., $Fe_4S_4L_n^-$ (L = Cl, Br, I) and $Fe_4S_n^-$ ($n = 4-6$), were mass-selected and decelerated before being intercepted by a probe laser beam in the detachment zone of the magnetic-bottle electron analyzer. The spectra of $Fe_4S_n^-$ ($n = 4-6$) from CID were measured for comparison with data taken with the laser vaporization cluster source. Two photon energies, 193 and 157 nm (7.866 eV), from an excimer laser were used for photodetachment on the CID products. Photoelectrons were collected at nearly 100% efficiency by the magnetic-bottle and analyzed in a 4 m long electron flight tube. Photoelectron time-of-flight spectra were collected and then converted to kinetic energy spectra, calibrated by the known spectra of I^- and O^-. The energy resolution ($\Delta Ek/Ek$) was about 2%, i.e., ~10 meV for 0.5 eV electrons, as measured from the spectrum of I^- at 355 nm.

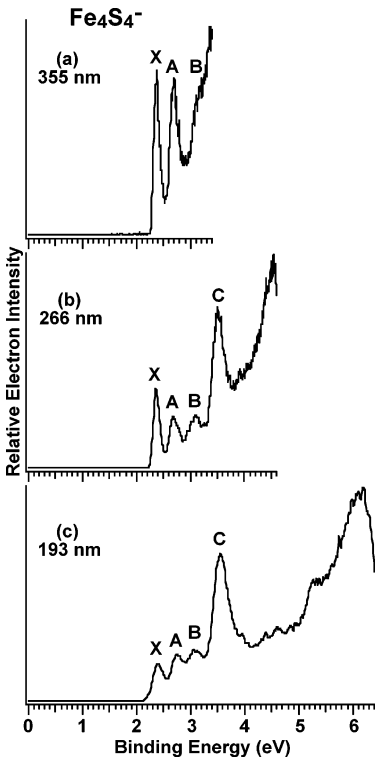

Figure 1. Photoelectron spectra of $Fe_4S_4^-$ at (a) 355 nm (3.496 eV), (b) 266 nm (4.661 eV), and (c) 193 nm (6.424 eV).

3. Results

3.1. PES of $Fe_4S_n^-$ ($n = 4-6$) Produced from Laser Vaporization. Photoelectron spectra of $Fe_4S_4^-$ at three photon energies are shown in Figure 1. The 355 nm spectrum (Figure 1a) revealed three bands (X, A, and B). The X band with a vertical detachment energy (VDE) of 2.37 eV was relatively sharp. Since no vibrational structures were resolved, the adiabatic detachment energy (ADE) was evaluated by drawing a straight line at the leading edge of the X band and then adding the instrumental resolution to the intersection with the binding energy axis. The well-defined onset of feature X allows a fairly accurate ADE of 2.30 ± 0.02 eV to be obtained, which represents the EA of the corresponding neutral Fe_4S_4 species. At 266 nm (Figure 1b), the B band was better defined, and another intense band C was revealed at 3.5 eV. The 193 nm spectrum (Figure 1c) showed the overall PES pattern of $Fe_4S_4^-$: three weak low binding energy bands (X, A, and B) followed by an intense and broader C band. The higher binding energy part of the 193 nm spectrum appeared to be continuous, indicative of the high density of electronic states.

The spectra of $Fe_4S_5^-$ and $Fe_4S_6^-$ are shown in Figure 2 at two photon energies. For $Fe_4S_5^-$, three well-defined bands (X, A, and B) were observed at 266 nm (Figure 2a); the A band overlapped with the more intense B band. The well-resolved X

(11) Yang, X.; Wang, X. B.; Niu, S. Q.; Pickett, C. J.; Ichiye, T.; Wang, L. S. *Phys. Rev. Lett.* **2002**, *89*, 163401.
(12) Yang, X.; Wang, X. B.; Wang, L. S. *Int. J. Mass Spectrom.* **2003**, *228*, 797.
(13) Wang, L. S.; Cheng, H. S.; Fan, J. *J. Chem. Phys.* **1995**, *102*, 9480.
(14) Wang, L. S.; Ding, C. F.; Wang, X. B.; Barlow, S. E. *Rev. Sci. Instrum.* **1999**, *70*, 1957.

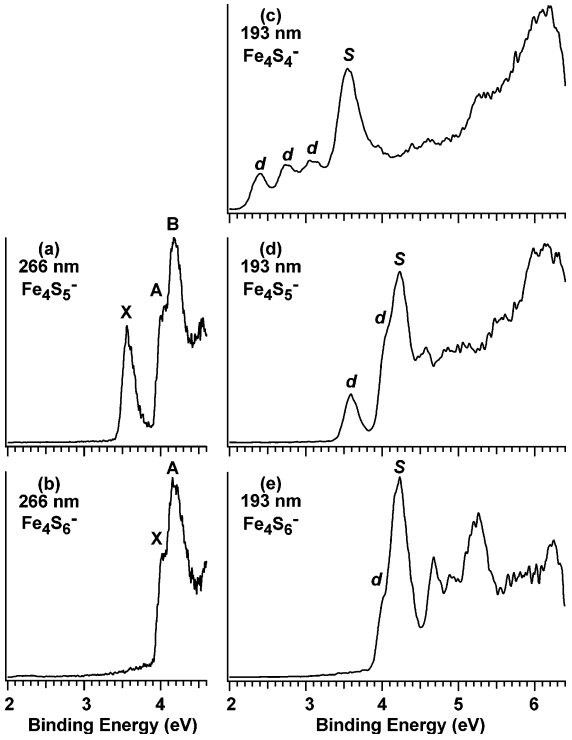

Figure 2. Photoelectron spectra of $Fe_4S_5^-$ and $Fe_4S_6^-$ at 266 and 193 nm. The 193 nm spectrum of $Fe_4S_4^-$ is compared with those of $Fe_4S_5^-$ and $Fe_4S_6^-$. The labels "d" indicate features from detachment of Fe 3d electrons, and "S" denotes features derived from S 3p-based molecular orbitals. See text for details.

band yielded a VDE of 3.56 eV and an ADE of 3.48 eV for the detachment transition from the ground state of $Fe_4S_5^-$ to that of Fe_4S_5. The ADE of $Fe_4S_5^-$ increased significantly compared to that of $Fe_4S_4^-$. The higher binding energy part of the $Fe_4S_5^-$ spectrum as revealed at 193 nm (Figure 2d) also appeared to be continuous. For $Fe_4S_6^-$, the 266 nm spectrum (Figure 2b) revealed two partially overlapped bands (X and A). An ADE of 3.94 eV was estimated from the sharp onset of band X, which also defined the EA of the Fe_4S_6 neutral cluster. The 193 nm spectrum revealed more well-defined features beyond 4.5 eV (Figure 2e).

The 193 nm spectrum of $Fe_4S_4^-$ is compared with those of $Fe_4S_5^-$ and $Fe_4S_6^-$ in Figure 2. The most remarkable feature in the three spectra is the intense band labeled as "S", meaning from S 3p derived molecular orbitals (MOs), as will be discussed later. The S band is similar in the three spectra and has the same VDE in the cases of $Fe_4S_5^-$ and $Fe_4S_6^-$. This band becomes the demarcation line in the spectra. Features to the left of the S band at lower binding energies are weaker in intensity and diminishes in numbers. These weak features are labeled as "d", meaning minority-spin Fe 3d derived bands. To the right of the *S* band at higher binding energies, all spectra became very complicated and only that of $Fe_4S_6^-$ exhibited resolved features. The binding energies of the spectra increase significantly, in particular from $Fe_4S_4^-$ to $Fe_4S_5^-$. The observed VDEs for the *d* and *S* features and the ground-state ADEs are given in Table 1.

3.2. $Fe_4S_4Cl_n^-$ (n = 3, 4). Under the CID conditions in our electrospray source, we were only able to observe the singly charged $Fe_4S_4Cl_4^-$ and its CID product by losing one Cl atom, $Fe_4S_4Cl_3^-$. The PES spectra of these two complexes at 193 and 157 nm are shown in Figure 3. The spectra of $Fe_4S_4Cl_4^-$

Table 1. Measured Adiabatic and Vertical Detachment Energies (eV) of the Low Binding Energy Features from the Photoelectron Spectra of $Fe_4S_n^-$ (n = 4−6) and $Fe_4S_4L_n^-$ (L = Cl, Br, I; n = 1−4)

			VDE[a]			
species	cubane core	ADE[a,b]	d band			S band
$Fe_4S_4^-$	$[Fe_4S_4]^-$	2.30 (2)	2.37 (2)	2.70 (2)	3.09 (2)	3.51 (2)
$Fe_4S_5^-$	$[Fe_4S_4]^+$	3.48 (2)	3.56 (2)	4.05 (3)		4.20 (2)
$Fe_4S_6^-$	$[Fe_4S_4]^{3+}$	3.94 (2)	4.05 (3)			4.20 (2)
$Fe_4S_4Cl_4^-$	$[Fe_4S_4]^{3+}$	4.62 (5)	4.85 (4)			5.56 (4)
$Fe_4S_4Cl_3^-$	$[Fe_4S_4]^{2+}$	4.23 (5)	4.42 (4)	4.74 (6)		5.20 (4)
$Fe_4S_4Br_4^-$	$[Fe_4S_4]^{3+}$	4.56 (5)	4.83 (4)			5.46 (4)
$Fe_4S_4Br_3^-$	$[Fe_4S_4]^{2+}$	4.23 (5)	4.41 (4)	4.72 (6)		5.15 (4)
$Fe_4S_4Br_2^-$	$[Fe_4S_4]^+$	3.76 (5)	4.08 (6)			4.70 (6)
$Fe_4S_4I_4^-$	$[Fe_4S_4]^{3+}$	4.47 (5)	4.70 (4)			5.24 (4)
$Fe_4S_4I_3^-$	$[Fe_4S_4]^{2+}$	4.20 (5)	4.36 (4)	4.65 (6)		5.01 (4)
$Fe_4S_4I_2^-$	$[Fe_4S_4]^+$	3.76 (5)	4.08 (4)			4.63 (4)
$Fe_4S_4I^-$	$[Fe_4S_4]^0$	3.03 (10)	3.23 (6)	3.62 (6)		4.36 (6)

[a] Numbers in parentheses represent experimental uncertainties in the last digits. [b] Also represent the adiabatic electron affinities of the corresponding neutral species.

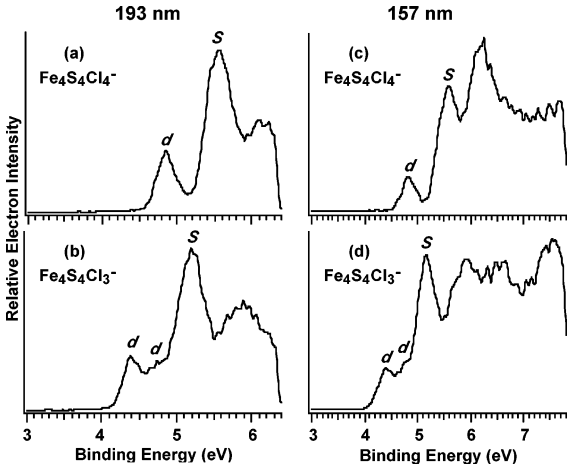

Figure 3. Photoelectron spectra of $Fe_4S_4Cl_n^-$ (n = 3,4) at 193 and 157 nm (7.866 eV). See Figure 2 cation for the labels "d" and "S".

displayed three features, labeled as d and S, as well as an intense band at 6.2 eV (Figure 3c). The d band had a relatively weak intensity and yielded a rather high ADE (4.62 eV) for $Fe_4S_4Cl_4^-$. The spectra of $Fe_4S_4Cl_3^-$ shifted to lower binding energies with an intense band labeled as S, which is similar to that in the spectra of $Fe_4S_4Cl_4^-$. There are two weaker features at the lower binding energy side, labeled as d. The separation between the first d band and the S band is almost identical to that in the spectra of $Fe_4S_4Cl_4^-$. With the exception of the extra d band in $Fe_4S_4Cl_3^-$, the overall PES spectral patterns of the two $Fe_4S_4Cl_n^-$ complexes are similar and they both also show some similarity to the spectra of the doubly charged $[Fe_4S_4Cl_4]^{2-}$ complex that we recently reported.[10] The ADEs for the first d band and the VDEs for all the d and S bands are given in Table 1.

3.3. $Fe_4S_4Br_n^-$ (n = 2−4). For the Br-ligated complexes, two CID products ($Fe_4S_4Br_3^-$ and $Fe_4S_4Br_2^-$) were observed under our experimental conditions. The PES spectra of $Fe_4S_4Br_n^-$ (n = 2−4) at 193 and 157 nm are shown in Figure 4. The spectra of $Fe_4S_4Br_4^-$ and $Fe_4S_4Br_3^-$ are nearly identical to those of the corresponding Cl-ligated complexes (Figure 3). The spectra of $Fe_4S_4Br_2^-$ shifted further to lower binding energies. The S band is similar to that in the spectra of $Fe_4S_4Br_3^-$, but the lower binding energy part of the $Fe_4S_4Br_2^-$ spectra seemed to be more complicated with unresolved bands, although only one d band

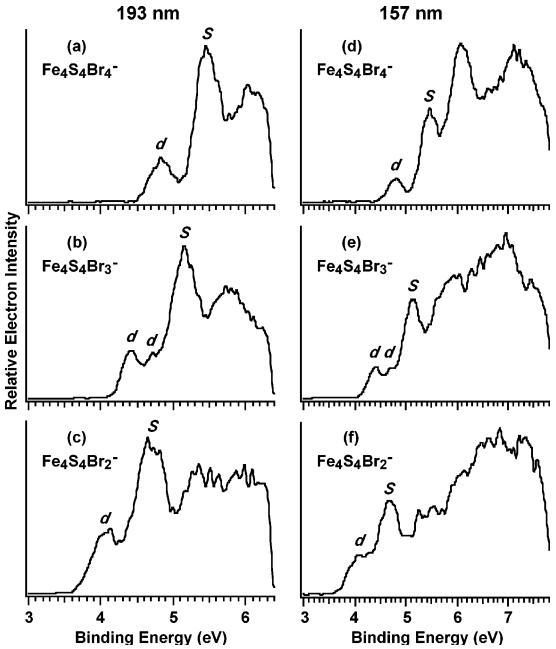

Figure 4. Photoelectron spectra of $Fe_4S_4Br_n^-$ ($n = 2-4$) at 193 and 157 nm. See Figure 2 cation for the labels "d" and "S".

was labeled. Again, the observed ADEs and VDEs are given in Table 1.

3.4. $Fe_4S_4I_n^-$ ($n = 0-4$). For the I-ligated cubane, the loss of all the ligands down to the bare $Fe_4S_4^-$ core was observed in the CID owing to the relatively weaker Fe−I bond. This series of complexes gave us the most systematic and complete data set, as shown in Figure 5. As n decreases, we observed that the spectra systematically shift to lower binding energies. For $n = 4$, 3, 2, the I-ligated complexes gave rise to similar spectra to those of the corresponding Br-ligated complexes. For $n = 1$ and 0, more d bands were observed at the lower binding energy side. Two were discernible in the spectra of $Fe_4S_4I^-$, and three in those of the bare $Fe_4S_4^-$. Although the higher binding energy side of the $Fe_4S_4^-$ spectra showed some difference, the spectra of $Fe_4S_4^-$ follow the general trend of the $Fe_4S_4I_n^-$ series, suggesting that the cubane core survived the CID processes and maintained a similar structure as that in the $Fe_4S_4I_n^-$ complexes. The ADEs and VDEs for the d and S bands of $Fe_4S_4I_n^-$ are also given in Table 1.

3.5. Comparison of the PES Spectra of $Fe_4S_n^-$ ($n = 4-6$) Produced from the Laser Vaporization and Electrospray Sources. In contrast to the intensive investigations on the [4Fe−4S] active sites in proteins and the cubane [4Fe−4S] cores in analogue complexes,[15−23] little is known about the bare $Fe_4S_4^-$cluster.[24,25] An interesting question concerns its ground state structure. Does it also possess a cubane-type structure?

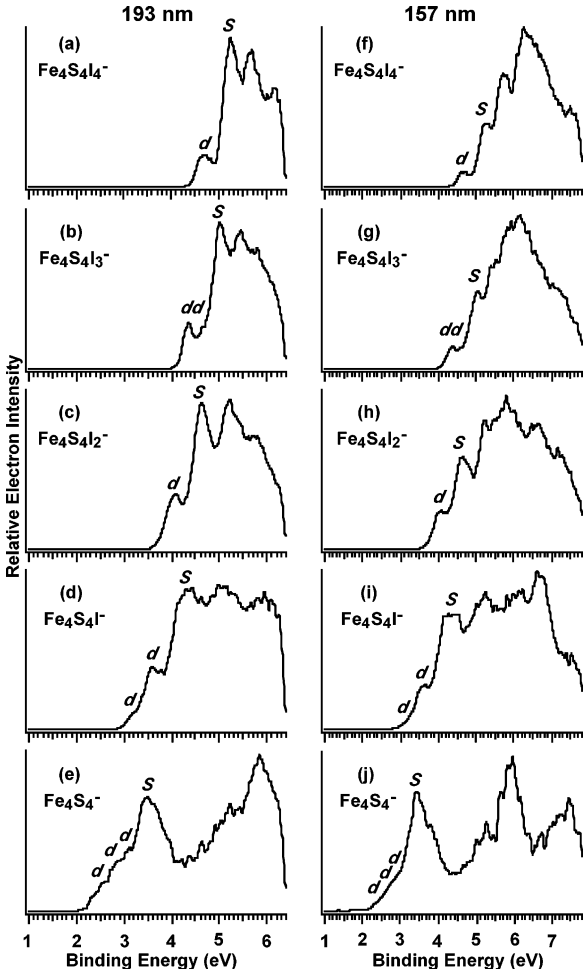

Figure 5. Photoelectron spectra of $Fe_4S_4I_n^-$ ($n = 0-4$) at 193 and 157 nm. See Figure 2 cation for the labels "d" and "S".

We were able to generate this cluster from both our laser vaporization and electrospray sources. The ion formation process is completely different in the two ion sources. In laser vaporization, clusters are formed through aggregation of atoms, and in general the lowest energy structures are produced.[26] On the other hand, the $Fe_4S_4^-$ clusters were formed by successive loss of the I ligands from $Fe_4S_4I_4^-$ through CID in the electrospray source. It was expected the cubane structure to be maintained, regardless if it is the lowest energy structure. The similarity and systematic trend in the complete data set shown in Figure 5 suggested that the cubane structure was intact in $Fe_4S_4^-$ produced by CID. Figure 6a and 6b compare the PES spectra of $Fe_4S_4^-$ produced from the two ion sources. They are essentially identical, except that the spectrum from the CID product was broader. The latter was due to the fact that the CID products were relatively hot with high internal energies, which could not be effectively cooled during the ion transport

(15) Holm, R. H. *Acc. Chem. Res*. **1977**, *10*, 427.
(16) Ogino, H.; Inomata, S.; Tobita, H. *Chem. Rev*. **1998**, *98*, 2093.
(17) Gebhard, M. S.; Deaton, J. C.; Koch, S. A.; Millar, M.; Solomon, E. I. *J. Am. Chem. Soc.* **1990**, *112*, 2217.
(18) Butcher, K. D.; Didziulis, S. V.; Briat, B.; Solomon, E. I. *J. Am. Chem. Soc*. **1990**, *112*, 2231.
(19) Butcher, K. D.; Gebhard, M. S.; Solomon, E. I. *Inorg. Chem*. **1990**, *29*, 2067.
(20) Gebhard, M. S.; Koch, S. A.; Millar, M.; Devlin, F. J.; Stephens, P. J.; Solomon, E. I. *J. Am. Chem. Soc*. **1991**, *113*, 1640.
(21) Glaser, T.; Rose, K.; Shadle, S. E.; Hedman, B.; Hodgson, K. O.; Solomon, E. I. *J. Am. Chem. Soc*. **2001**, *123*, 442.
(22) Kennepohl, P.; Solomon, E. I. *Inorg. Chem*. **2003**, *42*, 679.
(23) Harris, S. *Polyhedron* **1989**, *8*, 2843.
(24) (a) Nakajima, A.; Hayase, T.; Hayakawa, F.; Kaya, K. *Chem. Phys. Lett*. **1997**, *280*, 381. (b) Yu, Z.; Zhang, N.; Wu, X.; Gao, Z.; Zhu, Q.; Kong, F.; *J. Chem. Phys*. **1993**, *99*, 1765.
(25) Koszinowski, K.; Schroder, D.; Schwarz, H. *Eur. J. Inorg. Chem*. **2004**, 44.
(26) Comparisons between experimental photoelectron spectra and theoretical calculations have consistently revealed that the lowest energy structures were produced from the laser vaporization cluster source. For example, see: Akola, J.; Manninen, M.; Hakkinen, H.; Landman, U.; Li, X.; Wang, L. S. *Phys. Rev. B* **1999**, *60*, R11297. Li, X.; Kuznetsov, A. E.; Zhang, H. F.; Boldyrev, A. I.; Wang, L. S. *Science* **2001**, 291, 859. Li, J.; Li, X.; Zhai, H. J.; Wang, L. S. *Science* **2003**, 299, 864.

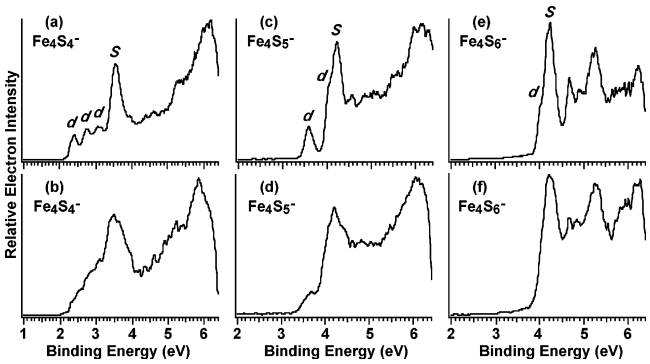

Figure 6. Comparison of photoelectron spectra of $Fe_4S_4^-$, $Fe_4S_5^-$, and $Fe_4S_6^-$ produced from two different ion sources. (Top) from laser vaporization of an Fe/S mixed target; (bottom) from collision-induced dissociation of doubly charged anions from an electrospray source.

and trapping. On the other hand, in the laser vaporization source the supersonic expansion provided moderate cooling and in general produces cluster anions with vibrational temperatures slightly below room temperature.[27] Thus, the identity of the PES spectra of $Fe_4S_4^-$ from two totally different formation processes indicated that the bare $Fe_4S_4^-$ cluster indeed possesses a cubane-like structure, probably not too different from that in the $Fe_4S_4L_4^-$ complexes.

We were also able to produce the $Fe_4S_5^-$ and $Fe_4S_6^-$ clusters from CID of $[Fe_4S_4(SC_2H_5)_4]^{2-}$ from our electrospray ion source. The PES data of these CID products are also compared to the data of the same species produced from laser vaporization in Figure 6. These two sets of data are again identical, except that the PES spectra from the CID products were broader analogous to the case of $Fe_4S_4^-$. The $Fe_4S_5^-$ and $Fe_4S_6^-$ CID products were formed by losing three and two $-SC_2H_5$ ligands and one and two $-C_2H_5$ units through S−C bond scission in the $-SC_2H_5$ ligand from a singly charged $Fe_4S_4(SC_2H_5)_4^-$ complex, respectively. The cubane core was expected to be intact in $Fe_4S_5^-$ and $Fe_4S_6^-$ from the CID, as in the $Fe_4S_4^-$ CID product from $Fe_4S_4I_4^-$. Therefore, the identity of the PES spectra of $Fe_4S_5^-$ and $Fe_4S_6^-$ produced from the two ion sources suggested that the ground state structures of these two clusters indeed contain an Fe_4S_4 cubane core and the extra S atoms can be considered as terminal ligands to the Fe_4S_4 core.

4. Discussion

4.1. PES Spectra of $Fe_4S_4L_4^-$ and $Fe_4S_6^-$ and the "Inverted Level Scheme" for the Cubane Core. In a recent study, we investigated the electronic structure of a series of doubly charged $[Fe_4S_4L_4]^{2-}$ analogue complexes with L = Cl, Br, I, SC_2H_5, and SH.[10] The PES data showed similar spectral patterns with each other and confirmed the "inverted level scheme" for the [4Fe−4S] cubanes,[28−31] as shown schematically in Figure 7a. In this model, the cubane complexes are viewed as a two-layer system (Figure 7b). Within each sublayer, the two high-spin Fe atoms are ferromagnetically coupled, and the two

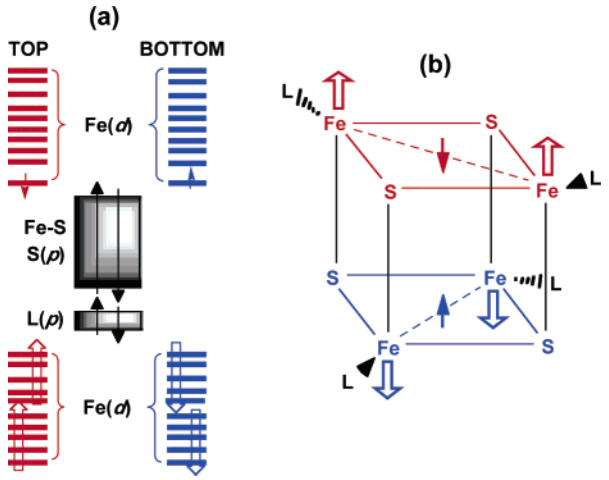

Figure 7. (a) Schematic of the inverted level scheme for an $[Fe_4S_4L_4]^{2-}$ complex with a $[4Fe-4S]^{2+}$ cubane core. (b) The two-layer model showing the spin-coupling in the $[4Fe-4S]^{2+}$ cubane core. The large hollow arrows represent the d^5 majority-spin electrons on each Fe, and the small arrows represent a single minority-spin electron delocalized over two Fe centers in each sublayer.

sublayers are coupled antiferromagnetically to give a low-spin state for the cubane complexes. There is a large spin polarization of the Fe 3d levels with the majority spin states stabilized over the minority spin states by ∼4−5 eV. The single minority spin in each sublayer is delocalized over the two Fe centers, giving rise to a formal oxidation state of $Fe^{2.5+}$. The Fe−S based orbitals and S(3p) lone pairs lie above the majority-spin levels but below the Fe(3d) minority-spin levels, giving rise to the inverted level scheme. In $[Fe_4S_4L_4]^{2-}$, there are two energetically equivalent minority spins, one in each [2Fe−2S] sublayer, whereas, in the singly charged $Fe_4S_4L_4^-$ complexes, there is only one minority-spin electron. The detachment of this electron gave rise to the weak d band in the PES spectra of $Fe_4S_4L_4^-$, as summarized in Figure 8a−c for L = Cl, Br, I. The second PES band (S) corresponds to detachment primarily from S-based MOs. We noted that the PES pattern of the $Fe_4S_4L_4^-$ singly charged species are very similar to those of the corresponding doubly charged $[Fe_4S_4L_4]^{2-}$ complexes,[10] except that the binding energy of the singly charged species is much higher due to the absence of the intramolecular coulomb repulsion present in the doubly charged anions.[32] The relative intensity of the first band is weaker in the PES spectra of the singly charged species than that observed for the doubly charged anions because this feature corresponds to only one minority-spin electron in the singly charged complexes. Therefore, our PES data of the singly charged $Fe_4S_4L_4^-$ complexes with a $[4Fe-4S]^{3+}$ oxidation state is consistent with the inverted level scheme shown in Figure 7a. All these complexes should have a spin of $^1/_2$, due to the presence of the single minority-spin electron.

The PES spectrum of $Fe_4S_6^-$ is compared to those of $Fe_4S_4L_4^-$ in Figure 8. As discussed above, this cluster is expected to have a cubane core with a $[4Fe-4S]^{3+}$ oxidation state. Although the spacing of the first two features in the PES spectrum of $Fe_4S_6^-$ (Figure 8d) is much smaller, their relative intensities are similar to that in the spectra of $Fe_4S_4L_4^-$. Thus, the weak low binding energy feature (d), which appeared as a shoulder, should correspond to the single minority-spin electron

(27) Wang, L. S.; Li, X. In *Clusters and Nanostructure Interfaces*; Jena, P., Khanna, S. N., Rao, B. K., Ed.; World Scientific: Singapore, 2000; pp 293−300.
(28) Noodleman, L.; Peng, C. Y.; Case, D. A.; Mouesca, J.-M. *Coord. Chem. Rev.* **1995**, *144*, 199.
(29) Aizman, A.; Case, D. A. *J. Am. Chem. Soc.* **1982**, *104*, 3269.
(30) Noodleman, L.; Norman, J. G.; Osborne, J. H.; Aizman, S.; Case, D. A. *J. Am. Chem. Soc.* **1985**, *107*, 3418.
(31) Torres, R. A.; Lovell, T.; Noodleman, L.; Case, D. A. *J. Am. Chem. Soc.* **2003**, *125*, 1923.
(32) Wang, L. S.; Ding, C. F.; Wang, X. B.; Nicholas, J. B. *Phys. Rev. Lett.* **1998**, *81*, 2667.

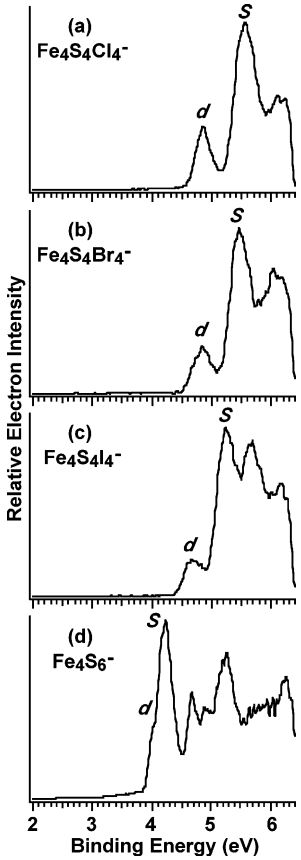

Figure 8. Comparison of photoelectron spectra of all species with a $[Fe_4S_4]^{3+}$ core.

in the $[4Fe-4S]^{3+}$ cubane core and the intense band (S) should correspond to S-based MOs (Figure 8d). Thus, the electronic structure of $Fe_4S_6^-$ can also be described by the inverted level scheme with a spin of $^1/_2$, similar to the $Fe_4S_4L_4^-$ complexes. The two extra S atoms most likely coordinate each to two Fe atoms in the two sublayers of the cubane core. The smaller d−S band spacing and the different spectral pattern in the higher binding energy part in the spectrum of $Fe_4S_6^-$ are due to the difference between the S ligand and the halogen ligands. We noted that the d−S band spacing decreases slightly from $Fe_4S_4Cl_4^-$ to $Fe_4S_4I_4^-$, as the terminal ligand becomes less electron-withdrawing from Cl to I. Sulfur as a divalent terminal ligand should be even less electron-withdrawing relative to I, and the smaller d−S spacing in $Fe_4S_6^-$ is consistent with this trend.

4.2. PES Spectra of $Fe_4S_4L_3^-$ (L = Cl, Br, I) and the Effects of the Partial Coordination on the Electronic Structure of the Cubane. The partially coordinated $Fe_4S_4L_3^-$ complexes contain a cubane core with a $[4Fe-4S]^{2+}$ oxidation state, which is similar to that in the $[Fe_4S_4L_4]^{2-}$ doubly charged complexes. However, in $Fe_4S_4L_3^-$ the two sublayers are no longer equivalent due to the absence of one ligand. This asymmetry should induce a splitting in the minority-spin levels, which are no longer equivalent energetically. The minority-spin level (the HOMO of $[Fe_4S_4L_4]^{2-}$) involves Fe−Fe bonding interactions and Fe−L antibonding interactions within each [2Fe−2S] sublayer.[10,28] It is expected that the minority-spin level in the sublayer with only one ligand should be energetically stabilized, and the one in the sublayer with two ligands should remain the same as in $[Fe_4S_4L_4]^{2-}$. A splitting of the minority-spin levels was indeed evident in the PES spectra of the three $Fe_4S_4L_3^-$ complexes, as summarized in Figure 9. More interestingly, the separation between the first d band and the S band are nearly identical in the spectra of $Fe_4S_4L_3^-$ and $[Fe_4S_4L_4]^{2-}$, in complete agreement with the inverted level scheme, suggesting that the first d band came from detachment of the minority-spin electron in the [2Fe−2S] sublayer with two ligands and the second d band derived from detachment of the minority electron in the sublayer with only one ligand.

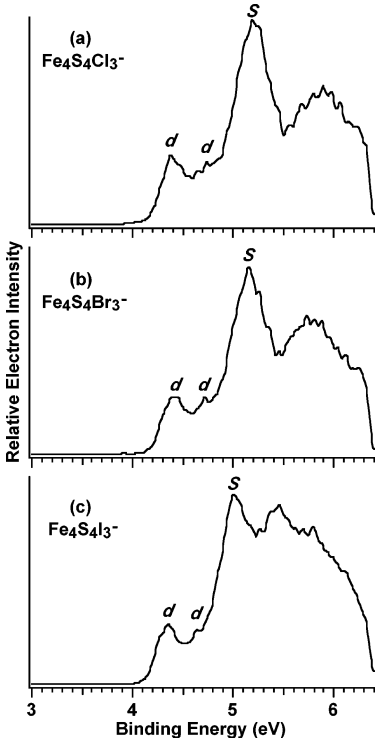

Figure 9. Comparison of photoelectron spectra of all species with a $[Fe_4S_4]^{2+}$ core.

4.3. PES Spectra of $Fe_4S_4L_2^-$ (L = Br, I) and $Fe_4S_5^-$. These three species should each contain a $[4Fe-4S]^+$ core with three minority-spin electrons. The spin coupling in these species is expected to be complicated and depends on how the two sublayers are divided, either as two [2Fe−2S−L] layers each coordinated with one ligand or one [2Fe−2S−2L] layer and one [2Fe−2S] layer without any terminal ligand. Either way, the two sublayers cannot be equivalent because of the odd number of the minority spin electrons, which should be distributed in the two sublayers as a 1 to 2 ratio (giving a spin $^1/_2$ state). Although only one d band is labeled in Figure 10a and 10b, the low binding energy parts of the PES spectra of $Fe_4S_4Br_2^-$ and $Fe_4S_4I_2^-$ were complicated and were not well resolved, suggesting perhaps a combination of all the above possibilities.

The PES spectrum of $Fe_4S_5^-$ is compared to those of $Fe_4S_4L_2^-$ in Figure 10. The low binding energy part of the $Fe_4S_5^-$ spectrum was much better resolved with two well-defined d bands. The extra S should coordinate to two Fe atoms in the $[4Fe-4S]^+$ core, defining one sublayer. The three minority spins may distribute similarly as in Figure 7b with two minority spins in the layer that is not coordinated by the fifth S atom, giving rise to a spin $^1/_2$ state for $Fe_4S_5^-$. The first d band in the PES spectrum of $Fe_4S_5^-$ then came from detachment of the highest occupied minority-spin electron. Dependent on the

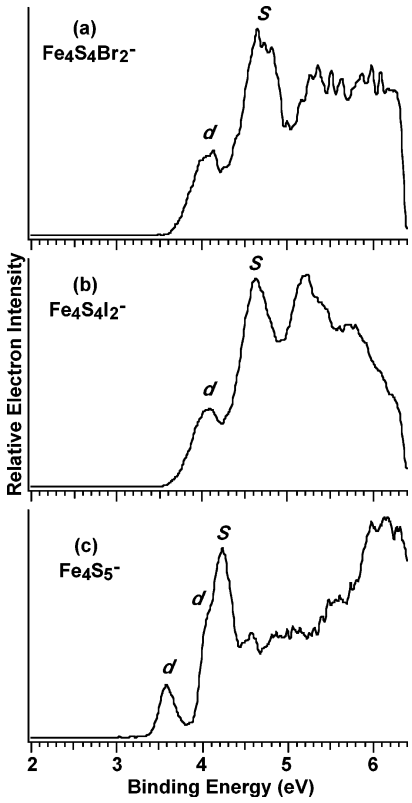

Figure 10. Comparison of photoelectron spectra of all species with an $[Fe_4S_4]^+$ core.

magnitude of the slitting between the two sublayers, either a spin 0 or a spin $^2/_2$ state can result for the ground state of neutral Fe_4S_5.

4.4. $Fe_4S_4I^-$ and $Fe_4S_4^-$. $Fe_4S_4I^-$ should contain a $[4Fe-4S]^0$ cubane core with four minority spins and all Fe are in the ferrous state. Thus each sublayer of the cubane core should have two minority-spin electrons, resulting in a spin 0 state for $Fe_4S_4I^-$. However, the two sublayers are inequivalent, which can result in a splitting of the minority-spin levels in the two sublayers, similar to the case in the $Fe_4S_4L_3^-$ complexes. This splitting was evident in the PES spectra of $Fe_4S_4I^-$ (Figure 5d and 5i). If the two sublayers were equivalent, two d bands would be expected with similar intensities. The low binding energy part of the PES spectra of $Fe_4S_4I^-$ was complicated, indicating more transitions were congested in this part of the spectrum and giving direct evidence for the splitting in the minority-spin levels due to the asymmetry of the coordination environment in $Fe_4S_4I^-$. The all-ferrous $[4Fe-4S]^0$ center of the Fe protein from *Azotobacter vinelandii* has been shown to have a spin state of $S = 4$ on the basis of Mössbauer and EPR studies.[33] One Fe site was shown to be unique presumably due to environmental or geometric asymmetries in the protein. This suggests that the two-layer model of the cubane as shown in Figure 7a is no longer applicable for the all-ferrous cubane.[31,33] The $Fe_4S_4I^-$ complex may be considered the simplest model system for the all-ferrous center because the single I ligand generates a unique Fe site naturally. Unfortunately, the current PES data are not sufficient to distinguish between the different spin states considered for the all-ferrous centers in the recent theoretical study.[31] Further theoretical study on the $Fe_4S_4I^-$ complex as a model for the all-ferrous $[4Fe-4S]^0$ center would be highly desirable.

There should be five minority spins in the bare $Fe_4S_4^-$ cluster. They should fill three levels in one sublayer and two in the other sublayer, according to the inverted level scheme of Figure 7a. This would result in a spin $^1/_2$ state for $Fe_4S_4^-$. Detachment from the highest occupied minority spin level gave rise to the X band in the PES spectra (Figure 1) and resulted in a spin 0 state for the ground state of neutral Fe_4S_4. Detachment from the other occupied minority spin levels would lead to either a spin 0 or spin $^2/_2$ excited state for neutral Fe_4S_4. If the splitting between these spin states is small relative to our spectral resolution ($\sim$30 meV in the relevant spectral range of Figure 1a), only one PES band would result. This indeed appeared to be the case, since only three well-resolved d bands (X, A, B) were observed in the PES spectra of $Fe_4S_4^-$ (Figure 1). Thus, our PES data suggested that the inverted level scheme devised for the cubane core is also applicable to describe the electronic structure of the bare $Fe_4S_4^-$ and Fe_4S_4 clusters.

4.5. Electron Storage and Sequential Oxidation of the [4Fe−4S] Cubane Cluster. Fe has two common oxidation states: Fe^{2+} and Fe^{3+}, which are cycled in redox reactions involving Fe. The strong spin polarization stabilizes the d^5 majority spins and destabilizes the single minority spin in the d^6 electron configuration of Fe^{2+}, making the Fe^{2+}/Fe^{3+} redox couple one of the most favorite in chemistry and biochemistry. The redox capability of all Fe−S clusters and proteins relies on this redox couple. In the cubane, the four Fe centers can store up to four minority-spin electrons in the all-ferrous $[4Fe-4S]^0$ oxidation states. In principle, all of these four electrons are available for electron-transfer reactions, leading to the all-ferric $[4Fe-4S]^{4+}$ oxidation state and giving the cubane cluster an extraordinary capacity for electron storage.

It is noteworthy that the bare Fe_4S_4 cluster possesses a cubane-type structure and its electronic structure can be described by the inverted level scheme (Figure 7a). This proves the stability of the cubane structural feature and provides further support for its robustness as a modular functional unit in analogue complexes and proteins. The fact that the bare $Fe_4S_4^-$ cluster possesses a cubane-type structure makes it possible for us to access the wide range of oxidation states of the cubane core in the gas phase. A recent density functional study investigated all five oxidation states of the analogue complex $[Fe_4S_4(SCH_3)_4]^{n-}$ ($n = 0-4$).[31] However, only the $n = 1$ and 2 species would be accessible in the gas phase, because the species with $n > 2$ would not be stable as gaseous species due to the strong intramolecular coulomb repulsion. The current investigation takes advantage of the variable terminal ligands to access a wide range of oxidation states for the cubane core all in the form of singly charged anions. Our recent study dealt with the doubly charged analogue complexes $[Fe_4S_4L_4]^{2-}$, which all contain a $[4Fe-4S]^{2+}$ cubane core.[10]

The $Fe_4S_4^-$ cluster in fact has five minority spins, even though this oxidation state is not accessible in either analogue complexes or proteins. In $Fe_4S_5^-$, two minority-spin electrons are transferred from the cubane core to the extra S, resulting in a $[4Fe-4S]^+$ oxidation state with three minority spins. In $Fe_4S_6^-$, a $[4Fe-4S]^{3+}$ oxidation is achieved. Thus from $Fe_4S_4^-$ to $Fe_4S_6^-$ a sequential oxidation of the cubane core is observed, and the

(33) Yoo, S. J.; Angove, H. C.; Burgess, B. K.; Hendrich, M. P.; Munck, E. *J. Am. Chem. Soc.* **1999**, *121*, 2534.

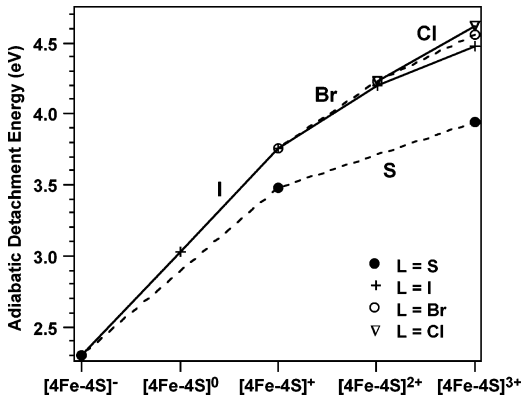

Figure 11. Adiabatic detachment energies vs the oxidation states of the [4Fe−4S] cubane core.

electron binding energies of the clusters also increase with the number of extra S ligands (Figure 2). Although the partially coordinated halogen complexes, $Fe_4S_4L_n^-$, were produced from the fully coordinated $Fe_4S_4L_4^-$, the series of species can also be viewed as a sequential oxidation of the cubane core from the bare $Fe_4S_4^-$ cluster because the core oxidation state increases by one with each additional halogen ligand in $Fe_4S_4L_n^-$. In the case of $Fe_4S_4I_n^-$, a full range of oxidation states of the cubane core is accessed from $[4Fe-4S]^- \rightarrow [4Fe-4S]^0 \rightarrow [4Fe-4S]^+ \rightarrow [4Fe-4S]^{2+} \rightarrow [4Fe-4S]^{3+}$ with $n = 0$, 1, 2, 3, and 4, respectively. The number of minority-spin electrons decreases from $5 \rightarrow 4 \rightarrow 3 \rightarrow 2 \rightarrow 1$ along the same sequence.

Figure 11 displays the ADEs of the threshold d band in the four series of $Fe_4S_4L_n^-$ species with respect to the formal oxidation states of the [4Fe−4S] cubane core. The ADEs represent the gas-phase oxidation potential of the corresponding complexes and increase in each series with the oxidation states of the cubane core. For the $[4Fe-4S]^{3+}$ core, the ADEs are extremely high, suggesting that it is much more difficult to oxidize the cubane core to the all-ferric form $[4Fe-4S]^{4+}$. The terminal ligands also have significant influences on the ADEs of the cubane complexes with the order S < I ≈ Br ≈ Cl. We observed that the extra S leads to a 1.18 eV increase of ADE in $Fe_4S_5^-$ relative to that in $Fe_4S_4^-$. This is almost twice as large an increase as the effect of two iodine atoms (Figure 11). This observation is consistent with the divalent nature of the extra S as terminal ligands in $Fe_4S_5^-$.

5. Conclusions

We report a photoelectron spectroscopic investigation of the electronic structure of the [4Fe−4S] cubane core with variable terminal coordination and oxidation states. Bare $Fe_4S_n^-$ ($n = 4-6$) clusters and synthetic analogue complexes $Fe_4S_4L_n^-$ (L = Cl, Br, I; $n = 1-4$) were produced by laser vaporization and electrospray ionization with CID and characterized by photoelectron spectroscopy. Photoelectron spectra of $Fe_4S_n^-$ ($n = 4-6$) produced from laser vaporization and CID confirmed that they all possess cubane-type structures with the extra S in $Fe_4S_5^-$ and $Fe_4S_6^-$ acting as terminal ligands to the cubane core. We found that the electronic structures of both the $Fe_4S_n^-$ and $Fe_4S_4L_n^-$ species can be described by the two-layer inverted level scheme. Five oxidation states of the cubane core, $[4Fe-4S]^- \rightarrow [4Fe-4S]^0 \rightarrow [4Fe-4S]^+ \rightarrow [4Fe-4S]^{2+} \rightarrow [4Fe-4S]^{3+}$, were accessed by varying the terminal ligand numbers. Spectral features due to the detachment of the minority-spin Fe 3d electrons were observed at the lowest binding energies and were readily recognized. Such 3d features decrease as the number of terminal ligands increases, i.e., the increase of the core oxidation states or the decrease of the number of minority electrons, revealing a behavior of sequential oxidation of the cubane core. Experimental evidence of the bare $Fe_4S_4^-$ cluster possessing the cubane-type structure proves the stability of the cubane structural unit. The behavior of sequential oxidation further confirms the electron-storage capability of the cubane core and its robustness as nature's favorite electron-transfer center.

Acknowledgment. We thank Prof. T. Ichiye and Dr. S. Niu for valuable discussions. This work was supported by the National Institutes of Health (GM-63555) and was performed at the W. R. Wiley Environmental Molecular Sciences Laboratory, a national scientific user facility sponsored by DOE's Office of Biological and Environmental Research located at Pacific Northwest National Laboratory, operated for DOE by Battelle.

JA0498437